Analytical Solutions of Some Cavity Creep Problems In Layered Salt Formations

H. A. M. van Eekelen
Koninklijke/Shell Exploratie en Produktie Laboratorium
Rijswijk, The Netherlands

ABSTRACT

This paper consists of two parts. In the first part, experimental results are given for the steady-state creep properties of the magnesium salts bischofite and carnallite. In the second part, analytical solutions are presented for three salt creep problems: borehole convergence, convergence of a spherical cavity and plastic salt influx into a cavity in a layered salt deposit. Results are supported by data from a limited number of field tests. From the three analytical solutions, tentative conclusions are drawn concerning the general dependence of cavity convergence rates on time, pressure and cavity geometry.

INTRODUCTION

In the vicinity of Veendam, the Netherlands, a solution mining program is in progress, designed to extract magnesium chloride from the salts deposited during the Zechstein stage. The magnesium chloride is mined from a layered deposit of halite (NaCl), carnallite ($KCl.MgCl_2.6H_2O$) and bischofite ($MgCl_2.6H_2O$). Some kieserite ($MgSO_4.H_2O$) and sylvite (KCl) are also present. The magnesium-containing layers are at a depth between 1400 and 2000 m, depending on precise location in a salt pillow. Production starts at the bottom of the magnesium salt layers, cavities being created in an upward direction, approximately 100 m wide and (ultimately) 100 m high.

Because carnallite and, especially, bischofite creep much more easily than halite, the criteria for stability of the Veendam cavities are qualitatively different from the criteria commonly used for halite caverns. First, the fluid pressure in the cavity and in the section of open hole above the cavity has to be maintained at such a level, close to lithostatic, that salt creep cannot endanger the integrity of the well tubulars. Second, when the cavity has been mined to its design limits, continued salt influx which occurs after abandonment (with attendant fluid loss from the cavity) could give rise to slow surface subsidence. Criteria must be developed to ascertain this risk and define measures to combat it.

In the first section of this paper, the results of creep tests on bischofite and carnallite are discussed. It is found that, in the strain rate range of interest, steady-state creep of these magnesium salts is described by a power law relation between stress and strain rate. In the next four sections this power law relation is applied to several salt creep problems. Explicit solutions are constructed, and from these solutions conclusions are drawn concerning the general dependence of cavity convergence rates on time, pressure and cavity geometry.

In the second section, basic flow equations are formulated and some simple approximations introduced. The third section gives an analytical solution for the case of salt creep into a borehole, and a comparison with the results of a small number of field tests. The fourth section gives a similar evaluation of creep convergence of a spherical cavity, and a discussion of the effect of cavity shape irregularity on cavity convergence. The fifth section contains an approximate analytical solution for the problem of squeezing creep of a bischofite or carnallite layer into a leaking abandoned cavity, followed by a discussion of time, pressure and geometry effects.

Finally, the last section gives the results of a recent decompression test on a halite/carnallite cavity in Veendam, and an interpretation in terms of elastic reaction, primary creep and secondary creep.

STEADY STATE CREEP TESTS ON BISCHOFITE AND CARNALLITE

In this section, a short review will be given of results obtained in three series of steady-state creep tests on

bischofite and one on carnallite. More detailed information on sample preparation, test equipment and loading procedures, and on part of the test results, has been given in ref. 1.

Sample Preparation

In most of the first and second series of tests on bischofite (van Eekelen et al, 1981), samples were obtained by milling core material to powder of less than 1 mm grain size, drying the powder at 25°C and 10% relative humidity, and compacting it for at least 12 hours in a 50.8 mm diameter vessel at a pressure of 35 MPa and a temperature of 110°C. The samples obtained in this way had a foam-like texture, with regularly shaped grains up to 2 mm in size. Instead of the core material, which also contained some carnallite and kieserite, a very pure, analytical grade of bischofite was also used. Moreover, some samples were obtained by slowly cooling a glass tube containing molten bischofite. Most samples had an estimated free water content of 0.1% by weight. This estimate was obtained by counting fluid inclusions on thin sections (see Figure 1d of van Eekelen et al., 1981). Samples with a free water content of 0.4% wt were obtained by adding one gram of water to 300 grams of dried bischofite powder; 'dry' samples with essentially zero free water content were made by adding 6 grams of tetrahydrate ($MgCl_2.4H_2O$) to 300 grams of dried bischofite powder.

A third series of tests on bischofite, and all tests on carnallite, have been performed on samples drilled directly from recent core material that had been cut and kept with utmost care and was in excellent condition. Samples were drilled from the core with a diamond drill cooled with *gas*

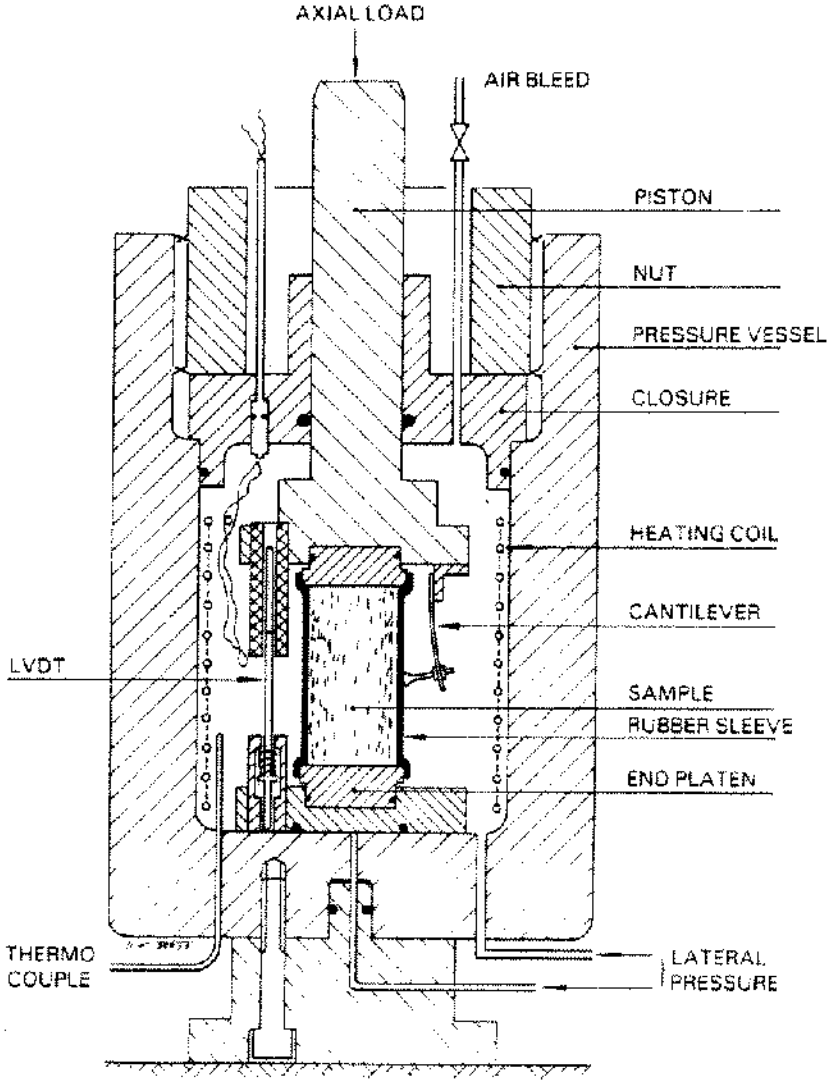

Figure 1. Triaxial cell for 2" × 4" samples.

oil (Kerosene), cleaned with pentane, and then stored in a dry room. Here the flat ends of the samples were ground parallel and covered with 0.1 mm thick teflon sheets and end platens. Butadiene sleeves were then fitted to the samples. Only then were the samples taken out of the dry room for testing. These precautions were necessary because carnallite and especially bischofite are very hygroscopic.

Test Equipment and Loading Procedures

Creep tests were performed in a standard triaxial cell, which had been provided with a heating coil and temperature control (Figure 1). End platens were made from a synthetic material with low thermal conductivity and were 10% oversize to allow for radial deformation of the samples. Axial load was applied by a load frame plus actuator, while confining pressure was supplied by the hydraulic oil in the cell. Axial deformation of the sample was measured with an LVDT of 20 mm range. Sample length was 101.6 mm, and diameter 50.8 mm.

Two loading procedures were used. In the first series of tests on bischofite and in all tests on carnallite, the strain rate was kept constant and the axial load was measured. In most other tests on bischofite the axial load was kept constant until steady-state creep had been obtained; the load was then changed and the creep rate determined at a new differential stress level. This method was employed to limit the number of samples used, and to partly eliminate the influences of differences in mechanical properties between different samples.

Test Results for Bischofite

In the first series of tests on bischofite, the effects of water content and impurity level were studied on compaction samples and melt samples, at a strain rate of 10^{-5}/s, a confining pressure of 28 MPa, and a temperature of 60°C. The main conclusions were the following (van Eekelen, *et al.*, 1981):

- For samples with a water content of 0.1-0.4% wt, steady-state creep was reached at a strain level of two or three percent, and the creep stress was independent of water content within this range. For dry samples a pronounced strain hardening was observed, and steady state creep had not been reached at ten percent strain.
- Pure bischofite samples (analytical grade) had a creep stress which was 10-30% lower than the creep stress for samples made from Veendam core material.
- Samples prepared by cooling molten bischofite were more coarse-grained than compaction samples and contained needles of tetrahydrate up to 5 mm long. Nevertheless, results on melt samples were in reasonable agreement with those on compaction samples.

In view of these results, and because *in-situ* bischofite was expected to have a free water content not less than 0.1% wt (see van Eekelen *et al.*, 1981), the second series of tests on bischofite were conducted on compaction samples with an estimated water content of 0.1%. The object of these tests was to produce data of secondary creep rate versus differential stress. Because temperatures in and around the Veendam cavities are between 50° and 80°C, the tests were performed at 40°, 60° and 80°C. Strain rates ranged from 10^{-5} to 2×10^{-8}/s, the latter being the lowest value of strain rate for which testing was practicable. Confining pressure was 28 MPa.

Results of this second series of tests are given in Figure 2 (three dashed curves). The straight line sections correspond to a power law relation between stress and strain rate (Appendix A):

$$\dot{\epsilon}_{ax} = \frac{2}{3} K (\Delta\sigma)^m \qquad (1)$$

where $\dot{\epsilon}_{ax}$ is the axial strain rate, and $\Delta\sigma$ is the difference between axial and lateral stress. Each of the straight lines is a least squares fit to at least six data points, the average value of the correlation coefficient r being 0.96. However, 20% of the original data set has been rejected in the fitting process, because measured strain rates deviated by more than a factor of 2.5 from the trends given by the remaining 80% of the data (see for example Figure 3).

Two types of bischofite creep can be distinguished, one operating at low strain rates and the other at high strain rates, with average values for m of 1.8 and 4.3, respectively (see Figure 2). With thin section microscopy it has been established that the dominant deformation mechanism at low strain rates is pressure solution plus grain boundary sliding, and at higher strain rates intracrystalline plastic flow assisted by dynamic recrystallisation (van Eekelen *et al.*, 1981; Urai, 1983).

Very recently, a third series of creep tests has been performed on bischofite samples drilled directly from new Veendam core material. The average free water content of these core samples was estimated (from thin sections) at 0.4% wt, with a lower limit of 0.1%. The results of these tests are represented by the two solid lines in Fig. 2. For 40°C, the agreement with the data on samples made by compaction of bischofite powder (in the high strain rate region) is good. For 60°C the agreement is reasonable, but for differential stress $\Delta\sigma < 3$ MPa, *the creep rate for the core samples is two to four times lower than for the compaction samples*. Also, the transition to 'low strain rate behaviour' is less distinct for the core samples; however, the number of low strain rate tests on core samples is rather limited (these tests are extremely time-consuming).

The full set of data points at 60°C is shown, together

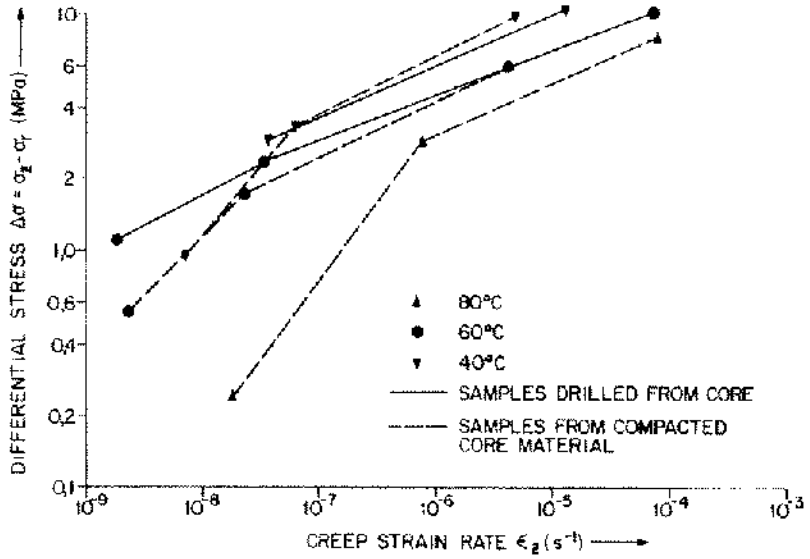

Figure 2. Triaxial test results for bischofite.

with the regression lines, in Figure 3. The values of m and K are, with time in seconds and stress in MPa:

$$\begin{array}{lll} \text{compaction samples} & m_1 = 2.00 & K_1 = 1.13 \times 10^{-8} \\ & m_2 = 4.24 & K_2 = 3.30 \times 10^{-9} \end{array} \quad (2)$$

$$\begin{array}{lll} \text{core samples} & m_1 = 3.93 & K_1 = 1.77 \times 10^{-9} \\ & m_2 = 5.28 & K_2 = 5.63 \times 10^{-10} \end{array} \quad (3).$$

These data will be used in the calculation of borehole convergence in section 4.

Test Results for Carnallite

Results of a series of tests on carnallite samples, drilled directly from Veendam core material, are given by the solid squares in Figure 4. These samples probably con-

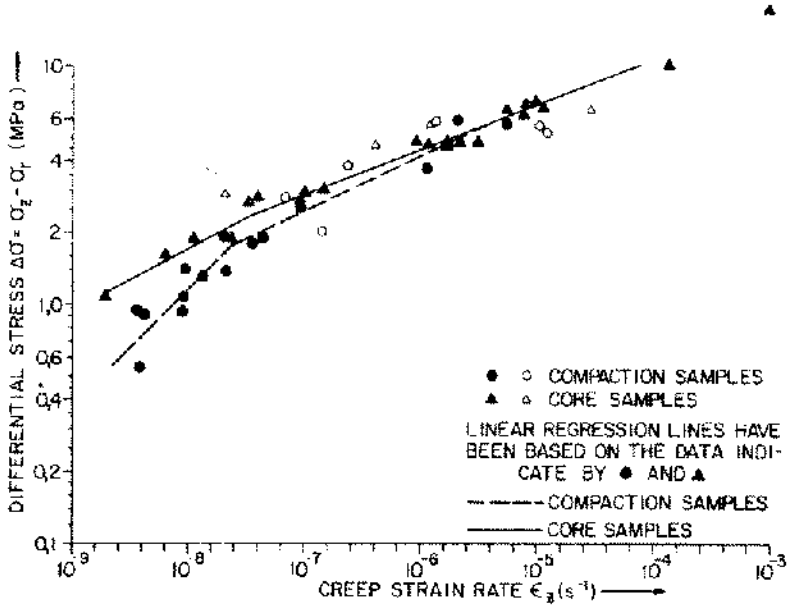

Figure 3. Creep rate versus differential stress for bischofite at 60°C.

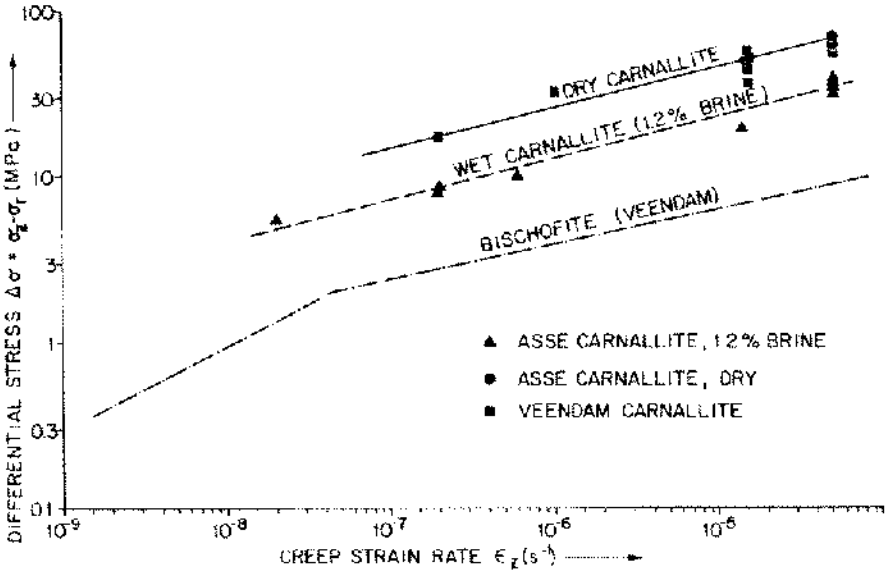

Figure 4. Creep rate versus differential stress for carnallite, at 60°C.

tained less than 0.1% wt free water. Also included in Figure 4 are results on Asse carnallite by Urai (1983), for dry samples and for samples to which 1.2% brine had been added (injected in the sleeve). The Veendam data are seen to agree with the data on dry Asse carnallite; the corresponding straight line in Figure 4 is given by

$$m_2 = 4.11 \qquad K_2 = 2.20 \times 10^{-12} \qquad (4).$$

At the same creep strain rate, creep stresses for dry carnallite are seen to be roughly seven times larger than for Veendam bischofite (in the high strain rate region). According to Urai (1983), for carnallite the transition to low strain rate behaviour is expected to occur at very low strain rates, of order 10^{-10}/s.

GENERAL EQUATIONS OF FLOW

The basic equations governing bischofite or carnallite creep are the mass balance

$$\text{div } \rho v + \partial\rho/\partial t = 0 \qquad (5),$$

the equation of motion or momentum balance

$$Dv/Dt = \rho g - \text{div } \sigma \qquad (6)$$

and the relation between stresses and (secondary) creep strain rates

$$\sigma = -2\eta\dot{\epsilon} + \frac{2}{3}\eta\, 1\, \text{trace}\, \dot{\epsilon} + p\, 1 \qquad (7).$$

In these equations, t is the time, v is the fluid (salt) velocity vector, ρ is the mass density of the fluid, p is the hydrostatic fluid pressure, g is the gravity acceleration vector, σ is the stress tensor (compression positive), $\dot{\epsilon}$ is the strain rate tensor (compression negative), and η is the (effective) fluid viscosity. Furthermore, 1 is the unit tensor,

$$\text{trace}\, \dot{\epsilon} = \text{div } v = \partial v_x/\partial x + \partial v_y/\partial y + \partial v_z/\partial z,$$

and Dv/Dt in Equation (6) is a 'material' derivative; it is the acceleration seen by an observer carried along by the flow.

The above constitutive Equation (7) already contains one approximation: elastic reaction and primary or transient creep of the salt have been neglected. Three more approximations will be introduced at this stage: neglect of fluid compressibility, fluid acceleration and gravity.

1. In general, the mass density of the fluid is related to the hydrostatic fluid pressure by the compressibility equation $\partial\rho/\partial p = \rho/K$ with K the compression modulus of the salt, which is roughly 25 GPa. Neglecting fluid compressibility leads to an error of order $\Delta P/K$ where, ΔP is a pressure difference relevant to the problem being studied (e.g., the difference between the fluid pressure in the borehole and the lithostatic pressure in the formation around the borehole). Because ΔP will be of order 10 MPa or smaller, the error involved in dropping fluid compressibility terms will be less than 0.1 of one percent.
2. If acceleration can be ignored, Equation (6) becomes the equation of force equilibrium. Dimensional analysis shows that neglect of acceleration terms leads to an error of order $\rho R^2 \Delta P/\eta^2$, where R is a characteristic length of the problem. From Fig-

ure 4 it can be seen that effective viscosities η are of order 10^5 MPa.s or much larger. Substituting $\rho = 1600$ kg/m^3, R = 50 m or smaller, and $\Delta P = 10$ MPa or smaller, one finds that the error involved in dropping acceleration terms is less than 0.4 of one percent. In actual cases the error is much smaller than that.

3. The gravity term ρg in Equation (6) is a so-called 'body-force field.' It does not represent the weight of the overburden, which enters our analysis as a boundary condition. Rather, it describes the differential stresses caused by the difference in mass density between salt and water or brine; in most cases, these stresses are very small and can be neglected. For a 10-m-high layer of bischofite, for instance, which adjoins a cavity or borehole filled with a brine of density 1.20, a gravity-induced differential stress of 0.02 MPa causes the bottom half of the layer to creep a littler faster than the top half. Because the effect is so small and of little interest to the problems being discussed in this paper, the gravity term in Equation (6) will also be neglected.

With the approximations given above, the flow equations simplify considerably, as follows:

$$\text{div } v = 0 \tag{8}$$

$$\text{div } \sigma = 0 \tag{9}$$

$$\sigma = -2\eta\dot{\varepsilon} + p1 \tag{10}.$$

It should be noted that, by the assumption of incompressibility, the fluid pressure p has become an 'indeterminate' quantity; it is no longer uniquely related to the state of compression of the material. Instead, it may be determined from the requirement that the solution of Equation (9) satisfy the constant volume condition Equation (8).

For a Newtonian fluid the viscosity η in Equation (10) is a constant. For our magnesium salts, however, the steady-state creep viscosity is strain-rate-dependent; in Appendix A it is shown that η may be expressed in the 'second invariant' $\dot{\varepsilon}_{eq}$ of the strain rate tensor $\dot{\varepsilon}$, and the power law parameters m and K of eq. (1), as follows:

$$2\eta = K^{-1/m}\,\dot{\varepsilon}_{eq}^{-1+1/m} \tag{11}.$$

Because $m > 1$, the viscosity decreases with increasing strain rate.

BOREHOLE CONVERGENCE

Salt deposits in Veendam consist of an alternating sequence of halite, carnallite and bischofite layers, the bischofite layers being up to 12 m thick. Because of the low viscosity of bischofite, these layers frequently cause stability problems in boreholes in the north of the Netherlands; cases of stuck pipe or buckled casing are relatively common.

Converging creep of bischofite into a borehole is characterised by the fact that the thickness of the bischofite layer is large, compared to the radius of the borehole (ratio of approximately 100:1). Therefore, it is obvious that a good approximation will be obtained by putting axial (vertical) velocities equal to zero, and calculating the radially inward flow of bischofite into the borehole as a plane strain problem. The error involved can be shown to be of order $(R/Z)^2$ with R the radius of the borehole and Z the thickness of the bischofite layer. Even for a badly washed-out hole, for instance, R = 1 m, this error is still less than one percent. In a plane strain description, the problem of flow into a borehole is characterised by four parameters:

R	the radius of the borehole,
ΔP	the pressure deficit in the borehole,
m,K	the power law parameters describing bischofite flow.

The pressure deficit ΔP is defined as the difference between the lithostatic pressure P_o in the bischofite, and the fluid pressure P_f inside the borehole: $\Delta P = P_o - P_f$. For dimensional reasons, the creep velocity U of the borehole wall must be given by an expression of the form

$$U = -a\,R\,K\,(\Delta P)^m \tag{12}$$

where a is a constant. By solving Equations (8) to (10) we shall obtain the value of this constant a; we shall also derive an expression for U in the case of a double creep law (Figure 3).

For cylindrical plane strain, flow Equations (8) to (10) become

$$\partial u/\partial r + u/r = 0 \tag{13}$$

$$\partial\sigma_r/\partial r + (\sigma_r - \sigma_\varphi)/r = 0 \tag{14}$$

$$(\sigma_r, \sigma_\varphi, \sigma_z) = p - 2\eta\,(\partial u/\partial r, u/r, 0) \tag{15},$$

where u is the outward radial velocity, and σ_r, σ_φ, σ_z are the radial, tangential and vertical (principal) stresses, respectively. For brevity, the stress Equations (15) have been written in condensed notation; for instance, the equation for the tangential stress is $\sigma_\varphi = p - 2\eta\,u/r$.

Equations (13) to (15) will first be solved for the case when the behaviour of the material is described by a single pair of power law parameters m and K. First, the mass or volume balance Equation (13) gives $u = X/r$, with $X < 0$ a function of time. From Appendix A one than obtains $\dot{\varepsilon}_{eq} = -\sqrt{3}\,X/r^2$; substituting this into Equation (11) for η, and inserting the result into Equation (15), one obtains

$$(\sigma_r, \sigma_\varphi, \sigma_z) = p - (b, -b, 0)\,r^{-2/m} \tag{16}$$

with

$$b = (1/\sqrt{3})\,(-X\sqrt{3}/K)^{1/m} \tag{17}.$$

Substitution of σ_r and σ_φ into the stress equilibrium Equation (14) yields a simple expression for $\partial p/\partial r$, which after integration gives

$$p = c - (m - 1)\, b\, r^{-2/m} \qquad (18).$$

The integration constants c and b or X are obtained from the boundary conditions: $\sigma_r = P_o$ at infinity, and $\sigma_r = P_o - \Delta P$ at the borehole wall; this gives $c = P_o$ and $b = (\Delta P/m)\, R^{2/m}$. This completes the solution of the problem. For the radial velocity u one finds $u = -R^2/rT_c$, where the characteristic time T_c for the cyclindrical influx problem is given by

$$\frac{1}{T_c} = \frac{1}{\sqrt{3}} \left(\frac{\sqrt{3}}{m}\right)^m K\, (\Delta P)^m \qquad (19).$$

The borehole-wall velocity is $U = dR/dt = -R/T_c$, which does indeed have the form given by the dimensional Equation (12). The strain rate at the borehole wall is $\dot{\varepsilon}_R = -1/T_c$, and the half-closure time of the borehole is given by $t_{1/2} = 0.69\, T_c$. For the stress field one obtains, in the same condensed notation as used in Equation (15):

$$(\sigma_r, \sigma_\varphi, \sigma_z) = P_o - (m, m - 2, m - 1)\, (R/r)^{2/m}\, \Delta P/m \qquad (20).$$

It should be noted that, if m is larger than 2, all three principal stresses decrease towards the borehole. This effect is due to the increasing strain rate, which causes a reduction in effective viscosity.

A very similar solution can be derived for the case where the salt obeys a double power law, with $m = m_1$, $K = K_1$ for $\dot{\varepsilon}_{eq} < \dot{\varepsilon}'$, and $m = m_2$, $K = K_2$ for $\dot{\varepsilon}_{eq} > \dot{\varepsilon}'$, where $\dot{\varepsilon}'$ is the value of $\dot{\varepsilon}_{eq}$ at the 'knee' (the transition from high strain rate to low strain rate behaviour) in Figure 3. For a sufficiently large pressure deficit ΔP, the flow field will then consist of an outer part where one has $m = m_1$ and $K = K_1$, and an inner part where $m = m_2$ and $K = K_2$. Because Equation (13) still gives $u = X/r$ and $\dot{\varepsilon}_{eq} = -\sqrt{3}X/r^2$, the boundary between inner and outer region falls at $r = R'$, with R' given by

$$-\sqrt{3}\, X/R'^2 = \dot{\varepsilon}' \qquad (21).$$

The stresses are again given by Equations (16) and (18), where now b, c, m and K have index 1 in the outer region and index 2 in the inner region. Substituting X from Equation (21) into the expressions for b_1 and b_2, Equation (17), the stresses become

$$(\sigma_r, \sigma_\varphi, \sigma_z) = c - (m, m - 2, m - 1)\, (R'/r)^{2/m}\, \sigma'/\sqrt{3} \qquad (22),$$

where c and m have index 1 and 2 in the outer and inner region, respectively. The stress σ' in eq. (22) is given by

$$\sigma' = \left(\frac{\dot{\varepsilon}'}{K_1}\right)^{1/m_1} = \left(\frac{\dot{\varepsilon}'}{K_2}\right)^{1/m_2} = \left(\frac{K_1}{K_2}\right)^{1/(m_2 - m_1)} \qquad (23).$$

The boundary condition for large r, $\sigma_r = P_o$, gives $c_1 = P_o$, and continuity of σ_r at $r = R'$ gives $c_2 = P_o - (m_1 - m_2)\, \sigma'/\sqrt{3}$. Finally, the boundary condition at the borehole wall, $\sigma_r = P_o - \Delta P$, gives an expression for R'. This completes the solution of the problem. For the radial velocity u one again finds $u = R^2/rT_c$, where the characteristic time T_c is now given by

$$\frac{1}{T_c} = \frac{1}{\sqrt{3}} \left(\frac{\sqrt{3}}{m_2}\right)^{m_2} K_2\, (\Delta P + (m_2 - m_1)\, \sigma'/\sqrt{3})^{m_2} \qquad (24)$$

where σ' is determined from Equation (23). Of course, this solution only applies if an inner region with $\dot{\varepsilon}_{eq} > \dot{\varepsilon}'$ does develop. If this is not the case, Equation (19) applies with $m = m_1$ and $K = K_1$. The condition for an 'inner region' to exist is that the pressure deficit ΔP in the borehole is larger than $m_1\, \sigma'/\sqrt{3}$. This may be derived by calculating the value of ΔP for which the two expressions for T_c become equal.

From the above solution, the half closure time $t_{1/2} = 0.69\, T_c$ of the borehole can be calculated as a function of the pressure deficit ΔP. The results for bischofite at 60°C are shown in Figure 5, where the dashed line is based on the data on compaction samples, Equation (2), and the full line is based on the core data of Equation (3). It is

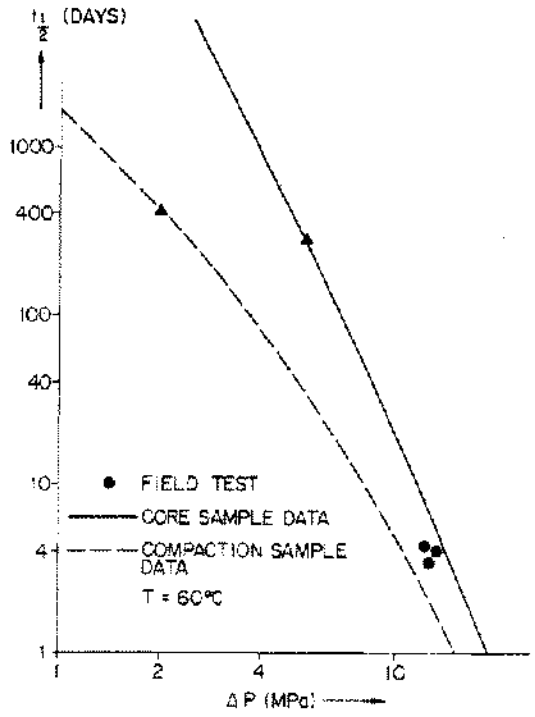

Figure 5. Half-closure times for a borehole in Bischofite. The triangles indicate the pressure deficit ΔP for which an "inner region" with $\dot{\varepsilon}_{eq} > \dot{\varepsilon}$ starts developing.

seen, for instance, that at a pressure deficit of 10 MPa, it takes 5 to 20 days for the borehole radius to be reduced to half its original value.

During a recent period of drilling in the Veendam area, borehole convergence tests were performed on three wells. The table below gives measured volume reductions over a time period Δt, and volume reductions calculated from data on compaction samples and on core samples.

Well nr	ΔP (MPa)	Δt (h)	Volume reductions in percent measured	calculated (core)	calculated (comp.)
1	12.6	49	57	34	75
2	13.2	10	14	10	29
3	12.2	29	33	19	52

Original borehole volumes were calculated from drill diameter (owing to the use of highly supersaturated mud the hole was very good on gauge), and borehole volume reductions were determined by BGL caliper. The pressure deficit ΔP was calculated from the overburden gradient (from density logs) and the mud weight.

As is already obvious, calculated convergence is very sensitive to the difference between the two data sets (Figure 5). Measured volume reductions fall approximately halfway between the two calculated values. Assuming that the borehole radius does indeed decrease exponentially with time ($R = R_0\, e^{-t/T_c}$), it is also possible to calculate half-closure times from the measured volume reductions and Δt. The results, plotted in Figure 5, again fall halfway between the two calculated curves.

CONVERGENCE OF A SPHERICAL CAVITY

By comparing the creep rate of a cylindrical cavity, as calculated in the General Equations section, with that of a spherical cavity in a homogeneous and infinitely large salt deposit, it is possible to obtain information on the influence of cavity shape on cavity convergence. For a spherical cavity, the flow Equations (8) to (10) become

$$\partial u/\partial r + 2u/r = 0 \qquad (25)$$

$$\partial \sigma_r/\partial r + 2(\sigma_r - \sigma_\varphi)/r = 0 \qquad (26)$$

$$(\sigma_r, \sigma_\varphi) = p - 2\eta(\partial u/\partial r,\ u/r) \qquad (27),$$

where u is the outward salt velocity, and σ_r and σ_φ are the radial and tangential stresses. These flow equations will be solved for power law material, with parameters m and K.

Equation (25) gives $u = X/r^2$, and hence $\dot{\epsilon}_{eq} = -3X/r^3$ (Appendix A). Substituting into Equation (11) and then into Equation (27), one finds

$$(\sigma_r, \sigma_\varphi) = p - (2b, -b)\, r^{-3/m}$$

with

$$b = \frac{1}{3}(-3X/K)^{1/m}$$

and, after substitution in Equation (26) and integration of the resulting expression for $\partial p/\partial r$,

$$p = c - (m - 1)\, 2b\, r^{-3/m}.$$

The boundary conditions at infinity and at the cavity wall give $c = P_0$ and $b = (\Delta P/2m)\, R^{-3/m}$, which completes the solution of the problem. For the radial velocity one obtains $u = -R^3/r^2 T_s$, where the characteristic time T_s for the spherical influx problem is given by

$$\frac{1}{T_s} = \frac{1}{3}\left(\frac{3}{2m}\right)^m K\,(\Delta P)^m \qquad (28).$$

For a cavity of volume V and arbitrary shape, we define the shape factor S as the convergence rate $-dV/dt$ of the cavity, divided by the convergence rate $-dV/dt = 3V/T_s$ of a spherical cavity of the same volume. For a cylindrical cavity one has $-dV/dt = 2V/T_c$, so that its shape factor becomes $S_c = 2T_s/3T_c$ or, using Equations (19) and (28)

$$S_c = (4/3)^{(m-1)/2} \qquad (29),$$

It should be noted that the shape factor is very sensitive to the value of m; from Equation (29) one has for a cylindrical cavity

$$S(m) = S(1)^{(m+1)/2} \qquad (30),$$

where S(1) is the shape factor for $m = 1$, which would apply for a Newtonian fluid (or for a linearly elastic solid).

We conjecture that the same relation between S(m) and S(1) will apply for a cavity of arbitrary shape. This would mean that cavity convergence by secondary creep would be much more sensitive to cavity shape irregularity than the primary elastic reaction of a cavity, especially if the cavity is in halite or carnallite, which (in the strain rate range of interest) have m roughly equal to 4.

THIN LAYER FLOW INTO A CAVITY

In this section we shall consider slow viscous flow of a relatively thin layer of bischofite or carnallite into a cavity, in which the fluid pressure is lower than the overburden pressure on the viscous salt layer. This situation arises, for instance, when, after abandonment (by cementation of the borehole), the cavity cannot hold a fluid pressure equal to the lithostatic pressure in the salt layer, and fluid leaks away at the casing shoe.

The geometry of the problem is illustrated in Figure 6. A cavity of radius R is surrounded by an elastic rock mass containing a viscous salt layer of thickness 2Z, with $Z \ll R$. The equilibrium lithostatic pressure in the salt layer is P_0. Originally, the fluid pressure in the cavity is also equal to P_0, but at time $t = 0$ it decreases to $P_0 - \Delta P$, with ΔP the cavity pressure deficit. This causes radial inflow of the salt, the viscosity of which is given by the power law parameters m and K. The surrounding rock

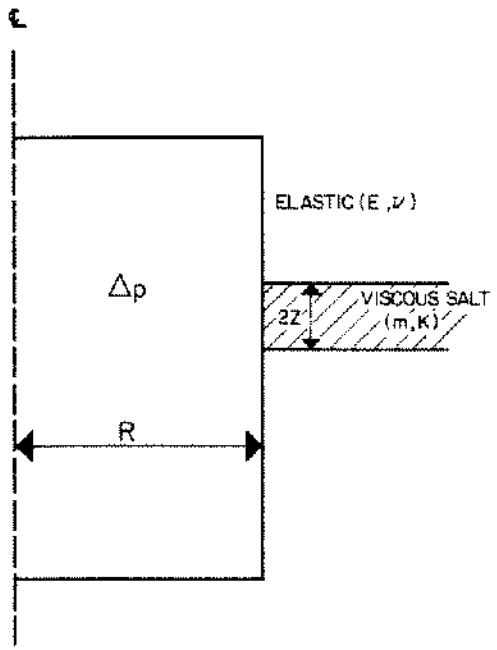

Figure 6. Geometry of thin-layer flow problem.

mass is supposed to be linearly elastic. This assumption is justified by the fact that the creep rate of halite is small compared with that of carnallite at the same differential stress, and both creep rates are small compared with that of bischofite; moreover, differential stresses will be small.

The problem of thin-layer flow is more complex than that of borehole or cavity convergence, since now the elastic moduli of the surrounding rock will affect the salt influx rate. Our reason for considering thin-layer flow is twofold:

- a rough estimate is wanted of the salt influx rate, since in the long run this process may cause surface subsidence, and
- we are interested in the effect of the surrounding elastic rock on the viscous salt flow. In particular, we want to know whether the salt influx rate will still be proportional to $(\Delta P)^m$, where m is the power law exponent of the viscous salt, or whether it will be proportional to a smaller power of the pressure deficit ΔP.

Because our objectives are qualitative rather than quantitative, our solution will only be a very approximate one. It will be assumed that the pressure gradient $\partial p/\partial r$ in the salt layer near the cavity wall is of the order of $\Delta P/R$ or smaller. This implies that the solution does not apply for very short times (this criterion will be quantified below). The fluid pressure field p [see Equation (10)] will then be mainly dependent on r and vary little through the thickness of the salt layer. Furthermore, the dominant velocity is the radial salt velocity u(r, z, t), and the dominant strain rate is the vertical derivative $\partial u/\partial z$ of u(r, z, t). Neglecting terms of the order of $(Z/R)^2$, the flow Equations (8) to (10) then simplify as follows: the stresses are given by

$$\sigma_r = \sigma_\varphi = \sigma_z = p$$

$$\tau_{rz} = -\eta\, \partial u/\partial z$$

and the only non-trivial force equilibrium equation is

$$\frac{\partial P}{\partial r} - \frac{\partial}{\partial z}\eta\frac{\partial u}{\partial z} = 0 \qquad (31)$$

with $p = p(r, t)$. Because the flow profile will be symmetrical around the plane $z = 0$ (see below), we need only consider u(r, z, t) in the region $0 \le z \le H(r, t)$, where $z = H(r, t)$ is the interface with the overlying rock. In this region, we have $u \le 0$, $\partial u/\partial z \ge 0$, $\partial u/\partial z = 0$ in $z = 0$, and $u = 0$ in $z = H$.

The viscosity η is given by Equation (11) with $\dot\epsilon_{eq} = 1/2\sqrt{3}\,\partial u/\partial z$ (see Appendix A). Substituting for η in Equation (31) and integrating over z, one obtains

$$\partial u/\partial z = 2\,K\,(\sqrt{3})^{m-1}\,z^m\,(\partial p/\partial r)^m.$$

By integrating over z twice, one obtains the total radial inflow Q(r, t) at $r \ge R$

$$Q(r, t) = -4\pi r \int_0^H u(r, z, t)\, dz$$

$$= 4\pi r\, K'\, H^{m+2}\,(\partial p/\partial r)^m \qquad (32),$$

where $K' = 2K\,(\sqrt{3})^{m-1}/(m+2)$. From conservation of mass one has, on the other hand,

$$Q(r, t) = 4\pi \int_r^\infty W(r', t)\, r'\, dr' \qquad (33),$$

where $W = -\partial H/\partial t$ is the downward velocity of the interface with the overlying rock. From Equations (32) and (33) one obtains a relation between the pressure gradient $\partial p/\partial r$ and the 'roof velocity' W

$$\left(\frac{\partial p}{\partial r}\right)^m = \frac{1}{H^{m+2}}\,\frac{1}{K'\,r}\int_r^\infty W(r', t)\, r'\, dr' \qquad (34).$$

At this stage, one needs a relation between the vertical roof displacement profile $Z = H(r, t)$ and the pressure field p(r, t) in the viscous salt layer. Here, we take a very simple approach. It will be assumed that the total thickness of the overburden is so large compared with the radius of the cavity, that the existence of a free ground surface does not affect our solution. The overburden, as well as the "underburden," will be represented by a homogeneous linearly elastic half-space with Young's modulus E and Poisson's ratio ν. The influence of the column of rock directly above and below the cavity will be neglected. In

general, the relation between $Z - H(r, t)$ and $p(r, t)$ may then be written as an integral equation

$$Z - H(r, t) = \frac{2(1 - \nu^2)}{E} \int_R^\infty K(r, r') \frac{\partial p(r', t)}{\partial r'} r' \, dr' \quad (35).$$

For $R = 0$, the integration kernel $K(r, r')$ is a known combination of elliptic integrals. One simple result is (Timoshenko and Goodier, 1951, section 124)

$$K(r, r') = 1 \qquad \text{for } r = R = 0 \quad (36).$$

For $R \neq 0$, it would be possible to derive a general expression for $K(r, r')$ and use this in a numerical solution of the problem. However, we are more interested in a simple approximate solution that provides physical insight and allows qualitative results to be derived. An alternative, much simpler approach has therefore been selected.

When at time $t = 0$ the pressure in the cavity has been lowered from P_o to $P_o - \Delta P$, a pressure disturbance starts propagating outward into the viscous salt layer. It will be assumed that at time t this disturbance has reached the point $r = R'(t)$

$$P_o - \Delta P \leq p(r, t) \leq P_o \qquad \text{for } R \leq r \leq R'(t)$$
$$p(r, t) = P_o \qquad \text{for } r \geq R'(t).$$

It will further be assumed that the roof displacement profile $Z - H(r, t)$ is a unique function of $x = r/R'$, $y = R'/R$, the pressure deficit ΔP, and the elastic constants E, ν, as follows:

$$Z - H(r, t) = \frac{2(1 - \nu^2)}{E} \Delta P \, R \, f(y) \, g(x) \qquad (R \leq r \leq R'(t)) \quad (37)$$

and

$$Z - H(r, t) = 0 \qquad (r \geq R'(t)).$$

The function $g(x)$ is a decreasing function of x, with $g(0) = 1$ and $g(1) = 0$, which gives a normalised roof sagging profile. The function $f(y)$ indicates how the roof sagging increases with time or with $y = R'/R$. The roof velocity $W(r, t)$ is obtained from Equation (37) by taking the derivative with respect to time t. Substituting the result into Equation (34) one obtains, at $r = \rho R < R'$

$$\left(\frac{\partial p}{\partial \rho}\right)^m = \frac{2(1 - \nu^2)\Delta P}{K' E} \left(\frac{R}{H}\right)^{m+2} \frac{dy}{dt} F(y, \rho) \quad (38)$$

where

$$F(y, \rho) = \frac{1}{\rho} \frac{\partial}{\partial y} [y^2 f(y) h(\rho/y)] \quad (39)$$

with

$$h(x) = \int_x^1 g(x') \, x' \, dx' \quad (40)$$

Equation (38) is an expression for the pressure gradient $\partial p/\partial \rho$ in terms of the functions $f(y)$ and $g(x)$, the penetration depth $y(t) = R'(t)/R$ of the pressure disturbance, and the elastic constants E, ν. From the fact that the total pressure increase from $r = R$ to $r = R'$ is equal to ΔP

$$\int_R^{R'} \frac{\partial p}{\partial r} dr = \int_1^y \frac{\partial p}{\partial \rho} d\rho = \Delta P \quad (41)$$

one may obtain an equation from which $y(t)$ can be solved. Substituting (38) into Equation (41) and replacing R/H by R/Z, where we use the assumption that $Z - H \ll Z$, we obtain

$$T_1 \, \phi(y) \, dy/dt = 1 \quad (42),$$

where

$$\phi(y) = \left[\int_1^y F(y, \rho)^{1/m} \, d\rho\right]^m \quad (43)$$

and

$$T_1 = \frac{2(1 - \nu^2)}{K' E (\Delta P)^{m-1}} \left(\frac{R}{Z}\right)^{m+2} \quad (44).$$

Integration of Equation (42) with $y(0) = 1$ gives the desired relation between the penetration depth $y(t) = R'(t)/R$ and the time t

$$t/T_1 = \int_1^y \phi(y') \, dy' \quad (45).$$

Substituting (38), with dy/dt given by Equation (42) into Equation (32), and putting $\rho = 1$, one obtains an expression for the salt influx rate into the cavity, $Q(t)$. By integrating this expression for $Q(t)$ over time, or by multiplying Equation (37) by r and integrating over r, the total influx $V(t)$ up to time t is obtained. The results, written in non-dimensional form, are

$$q \equiv \frac{T_2 \, Q(t)}{2\pi R^2 Z} = F(y, 1)/\phi(y) \quad (46)$$

$$v \equiv \frac{T_2 \, V(t)}{T_1 \, 2\pi R^2 Z} = y^2 f(y) h(1/y) \quad (47),$$

where

$$T_2 = \frac{1}{2K' (\Delta P)^m} \left(\frac{R}{Z}\right)^{m+1} \quad (48).$$

T_1 and T_2 are the two characteristic times of the problem. T_1 is the relaxation time of the viscoelastic system consisting of the viscous salt layer and the surrounding elastic rock, whilst $1/T_2$ is the characteristic strain rate for flow from the viscous salt layer under the cavity pressure deficit ΔP.

By inverting Equation (45) to give y as a function of t/T_1 and substituting the result into Equations (46) and (47), q and v are obtained as functions of t/T_1. These functions depend on the choice that is made for the functions f(y) and g(x) in Equation (37). However, this choice is not entirely free; it must satisfy the requirement that for $y \gg 1$ ($R' \gg R$, $t \gg T_1$) the roof displacement at the cavity wall given by Equation (37) approach the value given by the integral Equation (35) with $K(r, r') = 1$ and $\partial p/\partial r$ given by Equation (38). In Appendix B it is shown that for any given choice of the function g(x) this requirement is satisfied if for large y the function f(y) approaches γy, where γ is a numerical constant. Accordingly, we have taken $f(y) = \gamma y$ for all $y \geq 1$. For the normalised roof sagging profile g(x) with $g(0) = 1$ and $g(1) = 0$, we have made the simple choice

$$g(x) = (1 - x)^n \qquad (49).$$

Log v has been plotted against log t/T_1 (natural logarithms), for $n = 1, 2, 3$ and for the power law exponent m equal to 2 and 4 (Figure 7). From these results it can be seen that the choice of the function g(x) hardly affects the results of the calculation. We also expect the results to be insensitive to the precise choice for the function f(y), as long as $f(y) \to \gamma y$ for large y, and $f(y)\, g(\rho/y)$ is an increasing function of y for all values of ρ between 1 and y. [See Equation (37)]. The reason for this insensitivity is that in all cases the solution satisfies the requirements of conservation of mass and equilibrium of forces. The salt-influx rate is then largely determined by the creep properties of the salt, and the overall elastic behaviour of the surrounding rock mass, and (as long as $Z - H \ll Z$) less by the precise displacement profile of these rock masses.

In view of the results illustrated in Figure 7, we have selected the value $n = 2$ for the exponent in Equation (49). Log v has been plotted again versus log t/T_1, this time for $m = 2$, 3 and 4 (Figure 8). The straight lines in this plot are seen to give an excellent fit to the calculated results. Hence, we may write

$$v = v_1 (t/T_1)^{a_m} \qquad (50),$$

where v_1 is the value of v at time $t = T_1$, and (from Figure 8) $a_2 = 0.65$, $a_3 = 0.53$ and $a_4 = 0.43$; Equation (50) applies for values of t/T_1 between 1 and 10^5. It should be noted that, to a very good approximation, the above values for a_m may be written as $a_m = 2.6/(m + 2)$. [It can be shown that for very large values of t/T_1 the slope of the curves in Figure 7 and 8 asymptotically approaches $a = 3/(m + 2)$.] Using Equation (47), (48), (44) and (50), the total influx V(t) up to time t becomes

$$V(t) = \alpha\, t^a \left(\frac{1 - \nu^2}{E}\right)^{1-a} K^a (\Delta P)^{1+(m-1)a}\, R^{0.4}\, Z^{2.6} \qquad (51),$$

where α is a numerical constant which is roughly equal to 14.0. The influx rate Q(t) may be obtained from the relation $Q = aV/t$. From Equation (51) we arrive at the following conclusions.

1. When a cavity has a pressure deficit ΔP with respect to the equilibrium lithostatic pressure in a viscous salt layer, the salt influx from that layer goes with ΔP to the power $1 + (m - 1)\,a$, which is a substantially smaller exponent than the power-law exponent of the viscous salt itself. For instance, when $m = 4$, viscous inflow goes with ΔP to the power 2.3.

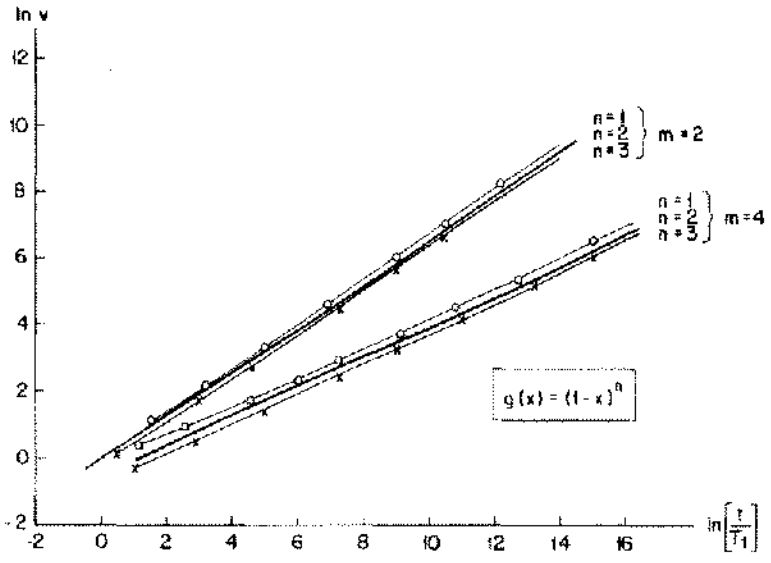

Figure 7. Bischofite flow into a cavity. Influx volume versus time, for three different sagging profiles.

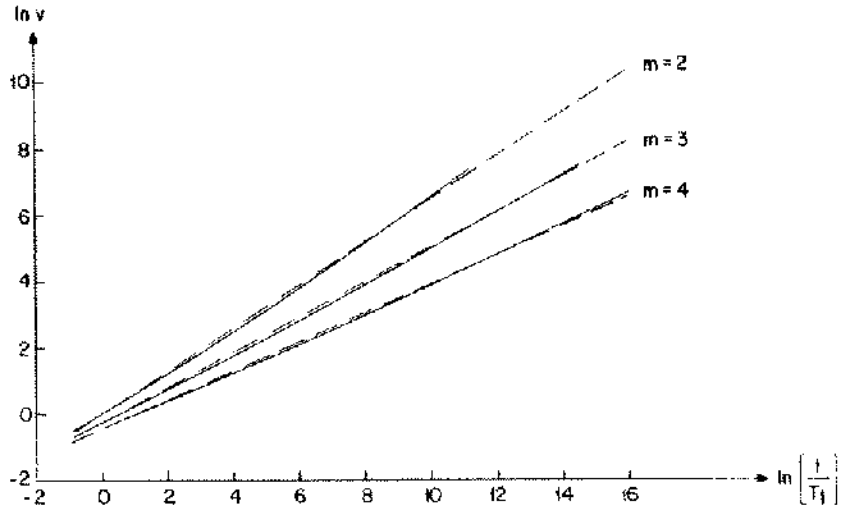

Figure 8. Bischofite flow into a cavity. Influx volume versus time, for three different values of m.

2. For a given cavity radius R, the salt-influx rate depends on the thickness 2Z of the viscous salt layer through a factor $Z^{2.6}$. On the other hand, for given layer thickness, the influx rate depends only weakly on the actual size of the cavity; V and Q are proportional to R to the power 0.4. It should be noted, however, that this (and any other) conclusion only applies if the cavity radius is much larger than the layer thickness, $R \gg Z$.
3. Even though the salt has been assumed to obey a steady-state creep law (deformation under constant differential stress proportional to time), the rate of salt influx into an underpressured cavity decreases with time to the power $-1 + a$. For instance, for m = 4 the influx rate goes with t to the power -0.57.

It should be noted that the solution to the thin-layer flow problem given by Equation (51) applies only to the case where the pressure deficit ΔP is constant in time. Also, the assumption made at the outset, that $\partial p/\partial r$ is of the order $\Delta P/R$ or smaller, limits the applicability to times t larger than T_f (see Appendix B). The assumption that the roof displacement $Z - H$ is much smaller than Z is satisfied for all practical cases.

One further remark should be made concerning the approximations made in this section. It has been assumed that the overlying rock mass could be represented by a homogeneous, infinitely high body of rock. If the cavity radius is much smaller than the distance to ground level, this assumption is correct for the initial stages of the influx process. However, as the pressure disturbance propagates to distances R′ much larger than the cavity radius R, the overburden will have a tendency to start behaving like a plate of finite thickness, and our solution will underestimate the salt influx into the cavity.

DECOMPRESSION FIELD TEST

In order to prevent bischofite or carnallite creep, cavities in Veendam are normally kept under pressure. Recently, however, one of the cavities was decompressed to hydrostatic (brine) pressure, to enable a workover to be performed. The cavity was in a layered deposit of halite and carnallite; no bischofite was present. During the decompression operation, cavity pressures were measured and efflux volumes recorded continuously. The results of the field test are given in Figure 9. The descending curve is the pressure in the cavity as a function of time; the equilibrium lithostatic pressure at the top of the precipitate layer in the cavity was estimated (from density logs) to be 31.6 MPa. The initial cavity pressure was 28.7 MPa.

The ascending full curve in Figure 9 gives the cumulative measured efflux volume. In general, the efflux is the sum of three contributions: an elastic reaction to any pressure decrease, a transient reaction to any pressure decrease, and a "steady" efflux due to the total cavity pressure deficit. The existence of transient phenomena can be observed from the records of the three periods S1, S2 and S3 during which the cavity pressure was kept constant. During these periods the efflux rate decreased until a more or less constant value was obtained. The transient contribution is probably due to primary creep of the salt; from the efflux records during the three periods of stable pressure the relaxation time of the primary creep phenomenon was estimated at 20 hours. The efflux rate at the end of the three periods should represent secondary creep of the salt. By plotting these efflux rates against the cavity pressure deficit during the periods on a log log scale (see insert in Figure 9) it was established that the steady efflux rates depended on ΔP to the power 2.17. Because carnallite has a power law index m of roughly 4

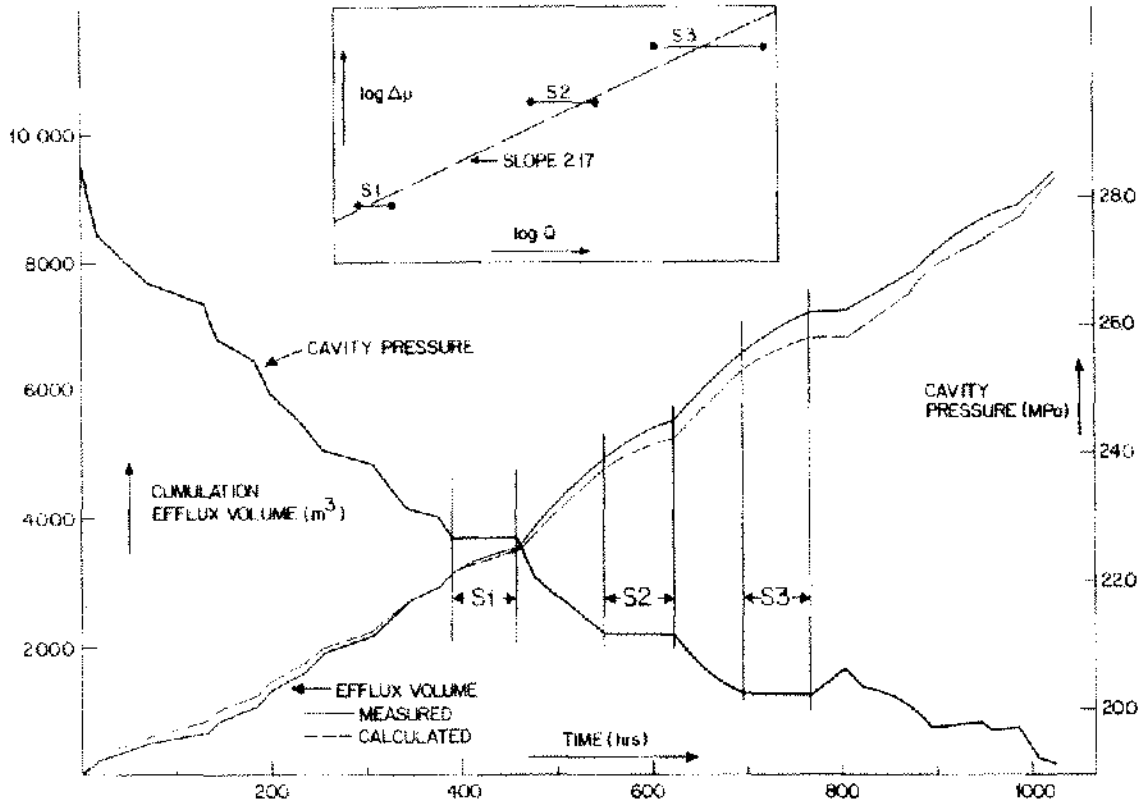

Figure 9. Decompression of a Carnallite/Halite cavity in Veendam. Insert: steady state flow rate Q versus cavity pressure deficit Δp.

(see section on Steady State Creep Tests), this result agrees with conclusion 1 in the section on Thin Layer Flow, even though not all of the conditions for the theory of that section to apply are met in this case.

The dashed line in Figure 9 is the best fit to the experimental efflux volumes that could be obtained with an empirical model, which contained an elastic term, a primary (transient) creep term and a secondary (steady state) creep term. Obviously, in view of the layering of the structure and the complicated shape of the cavity (which was largely unknown) it was not useful to try to describe the convergence of the cavity with a more sophisticated model. The transient relaxation time was taken as 20 hours, and the steady flow exponent was given the value 2.17. Four other parameters in the model were varied to obtain a good fit to the data.

The value obtained for the elastic modulus of the cavity corresponds with a value of G/S(1) of 2.8 GPa, where 1/G is the average shear compliance of the salt around the cavity, and S(1) is the linear shape factor introduced in section 5. A good mean value for the shear modulus of halite is 11 GPa (Hansen et al., 1981), while from our tests on carnallite we find a carnallite shear modulus of roughly 2 GPa. These data would give a G value of 3.4 GPa, which leads to the conclusion that the shape factor of the cavity would be of the order S(1) = 1.2. This result is not unreasonable.

CONCLUSIONS

1. The steady-state creep behaviour of carnallite is given by a power law with exponent $n = 4$, at least for strain rates down to 10^{-9}. Bischofite obeys a 'double' power law based on two different deformation mechanisms, with n equal to 4 or 5 in the high strain rate region; for strain rates lower than 2×10^{-8} the value of n is substantially lower.

2. Analytical expressions have been derived for the rate of closure of a borehole in carnallite or bischofite. For bischofite, there is reasonable agreement with the results of three recent field tests on borehole convergence.

3. Cavity convergence by secondary creep is a strongly increasing function of cavity shape irregularity. This applies especially for cavities in carnallite and/or halite.

4. If a cavity in a layered salt deposit (e.g., halite and carnallite, or carnallite and bischofite) has an internal fluid pressure that is lower than the lithostatic pressure, the salt influx from the more plastic salt layers will go with a power of the pressure deficit which is much smaller than the power-law exponent of this salt. This is con-

firmed by a recent decompression test of a Veendam cavity.

5. The rate of salt influx will be a strongly increasing function of the characteristic thickness of the plastic salt layers but will be almost independent of cavity volume. It decreases roughly with the square root of time.

Conclusions 4 and 5 apply only in those cases where the radius of the cavity is much larger than the thickness of the plastic salt layers.

REFERENCES

Hansen, F. D., K. D. Mellegard and P. E. Senseny, 1981. Elasticity and strength of ten natural rock salts. In Proceedings of the first conference on the mechanical behaviour of salt, State College, Pennsylvania, November (Trans Tech Publications, 1984).

Timoshenko, S. and J. N. Goodier. 1951. 'Theory of Elasticity'. McGraw Hill Book Company, New York, (2nd edition).

Urai, J. L. 1983. Ph.D. thesis, University of Utrecht, the Netherlands.

Urai, J. L. 1983. 'Water weakening and dynamic recrystallisation in polycrystalline Bischofite'. Tectonophysics. g6, pp. 125–151.

van Eekelen, H.A.M., A. Hulsebos and J. L. Urai. 1981. 'Creep of Bischofite'. In: Proceedings of the first conference on the mechanical behaviour of salt, State College, Pennsylvania, November 1981 (Trans Tech Publications, 1984).

APPENDIX A

The deviatoric stress tensor $\mathbf{s}$ is defined as follows:

$$\mathbf{s} = \sigma - \frac{1}{3}\mathbf{I}\,\text{trace}\,\sigma \qquad \text{(A1)},$$

where trace σ is the sum of the diagonal components of σ. The 'second invariant' σ_{eq} of the stress tensor σ is given by

$$\sigma_{eq} = \left(\frac{3}{2}s_{ij}s_{ij}\right)^{1/2} \qquad \text{(A2)}.$$

The second invariant $\dot{\epsilon}_{eq}$ of the strain rate tensor $\dot{\epsilon}$ is given by

$$\dot{\epsilon}_{eq} = \left(\frac{3}{2}\dot{\epsilon}_{ij}\dot{\epsilon}_{ij}\right)^{1/2} \qquad \text{(A3)},$$

where the salt has been assumed incompressible (trace $\dot{\epsilon} = 0$) (see section on General Equations). For an incompressible power law fluid, the relation between stresses and strain rates is

$$\dot{\epsilon} = -K\sigma_{eq}^{m-1}\mathbf{s}$$

and hence

$$\dot{\epsilon}_{eq} = K\sigma_{eq}^{m} \qquad \text{(A4)}.$$

From Equation (10) in the General Equations section we have, on the other hand, $\sigma_{eq} = 2\eta\dot{\epsilon}_{eq}$, so that the equivalent viscosity η is given by

$$2\eta = \sigma_{eq}/\dot{\epsilon}_{eq} = K^{-1/m}\dot{\epsilon}_{eq}^{-1+1/m}$$

which is Equation (11) of the General Equations section.

For a triaxial test one obtains, from Equation (A1), (A2) and (A3), $\sigma_{eq} = |\sigma_z - \sigma_r|$ and $\dot{\epsilon}_{eq} = |\dot{\epsilon}_z - \dot{\epsilon}_r|$. For triaxial compression this gives $\sigma_{eq} = \Delta\sigma$ and $\dot{\epsilon}_{eq} = 3\dot{\epsilon}_{ax}/2$, and substitution into Equation (A4) yields Equation (1) of the section on Steady State Creep Tests. The equivalent relation for triaxial extension is

$$\dot{\epsilon}_{ax} = -\frac{2}{3}K(-\Delta\sigma)^m.$$

Hence, for this power law model, the relation between differential stress and strain rate is the same for triaxial compression and for triaxial extension.

We finally derive the expressions for $\dot{\epsilon}_{eq}$ used in the Borehole, Convergence, and Thin Layer Flow sections. For cylindrical plane strain (Borehole section) one has $u = X/r$, and hence

$$\dot{\epsilon}_r = \partial u/\partial r = -X/r^2, \qquad \dot{\epsilon}_\varphi = u/r = X/r^2$$

and substitution into Equation (A3) gives $\dot{\epsilon}_{eq} = -\sqrt{3}\,X/r^2$. For spherical inflow (Convergence section), the radial velocity is $u = X/r^2$, and the strain rate components are

$$\dot{\epsilon}_r = \partial u/\partial r = -2X/r^3, \qquad \dot{\epsilon}_\varphi = \dot{\epsilon}_\theta = u/r = X/r^3$$

and substitution into Equation (A3) gives $\dot{\epsilon}_{eq} = -3\,X/r^3$. For thin layer flow (Thin Layer Flow section), the dominant strain rate is

$$\dot{\epsilon}_{rr} = \dot{\epsilon}_{zr} = \frac{1}{2}\partial u/\partial z,$$

and substitution into Equation (A3) gives $\dot{\epsilon}_{eq} = 1/2\sqrt{3}\,|\partial u/\partial z|$.

APPENDIX B

Notes on the thin-layer flow model

For the model of the thin layer flow section, we have from Equation (38), (42) and (44) the following expression for the radial derivative of the pressure p

$$\partial p/\partial\rho = \Delta P[F(y, \rho)/\phi(y)]^{1/m} \qquad \text{(B1)}.$$

For very large values of y, the roof displacement at the cavity wall, as given by Equation (37), must approach the value given by the integral expression (35), with $K(r, r') = 1$. Substituting $\partial p/\partial r$ from Equation (B1) into Equation (35), one obtains the condition

$$\lim_{y\to\infty}\frac{1}{f(y)}\left[\int_1^y F(y, \rho)^{1/m}\rho d\rho\right] \Big/ \left[\int_1^y F(y, \rho)^{1/m} d\rho\right] = 1,$$

Using expression (39) for $F(y, \rho)$ and substituting $f(y) = \gamma y$, one finds that this condition is satisfied if

$$\gamma = \left[\int_0^1 \psi(x)^{1/m}x^{1-1/m}dx\right] \Big/ \left[\int_0^1 \psi(x)^{1/m}x^{-1/m}dx\right],$$

where $\psi(x) = 3h(x) - x^2g(x)$ is a finite, decreasing function of x for $0 \le x \le 1$. The integrals in the right hand side are finite if $m > 1$, so that γ is a finite number and our asymptotic condition on the roof displacement is satisfied.

It has also been assumed that $\partial p/\partial r < \Delta P/R$ at $r = R$. From Equation (B1) and (46) one finds that the condition for this to be true is that $q = T_1\,dv/dt < 1$. Substituting Equation (50) for v, one finds that this condition is satisfied for $t/T_1 > 0.30$.